Lifetime Estimation of Cr_2AlC MAX Phase Foam Based on Long-Term Oxidation and Fracture Mechanisms

Wakako Araki[a,*], Asato Matsumoto[a], Yoshio Arai[a], Noriyasu Yamada[a], Jürgen Malzbender[b], and Jesus Gonzalez-Julian[b,c]

[a] Department of Mechanical Engineering, Saitama University, Japan

[b] Forschungszentrum Jülich GmbH, Institute of Energy and Climate Research, 52425 Jülich, Germany

[c] Department of Ceramics and Refractory Materials, Institute of Mineral Engineering, RWTH Aachen University, 52064 Aachen, Germany

* Corresponding author. araki@mech.saitama-u.ac.jp (W. Araki); email: araki@mech.saitama-u.ac.jp

ABSTRACT (250)

Oxidation kinetics and mechanical behaviour of Cr_2AlC foam with a porosity of 53 vol.% were investigated. Microstructures of Cr_2AlC foams oxidised in the temperature range 1173 to 1473 K for times between 0 and 100 h were examined. Uniaxial compression tests were performed at different temperatures in the range 298 to 1398 K to assess mechanical properties. The oxidation forms continuous with cohesive Al_2O_3 layers on the Cr_2AlC matrix, beneath which porous Cr_7C_3 is formed. The oxidation kinetics can be expressed by a parabolic law. An excessive oxidation takes place first in thin struts, where a breakage Al_2O_3 layer occurs, followed by oxygen inflow and decomposition of inner material. At 298 K, non-oxidised Cr_2AlC foam fractures intergranularly. Slight oxidation improves compressive strength, as the Al_2O_3 layer (2.5 μm or thinner) can prevent cracks to propagate from inside outward. However, an excessive oxidation deteriorates any improvement due to the breakage of Al_2O_3 layer in thin struts followed by the material decomposition. At 1273 K and 1398 K, non-oxidised porous Cr_2AlC fractures intergranularly, accompanied by a plastic deformation around small Al_2O_3 particles segregated at grain boundaries. Oxidised Cr_2AlC foam with the Al_2O_3 thickness of 2.5 μm has a slightly higher brittle-to-plastic transition temperature (~1273 K) than dense Cr_2AlC. A thicker Al_2O_3 layer (~5 μm) is required to reinforce the material due to inferior mechanical properties of Cr_2AlC at high temperatures. On the basis of the elucidated oxidation and fracture mechanisms, a safety criterion for high-temperature applications is suggested.

Keywords: MAX phases; Cr_2AlC; Mechanical properties; Porous materials; Oxidation; Lifetime

1. Introduction

MAX phases are layered materials with a general formula of $M_{n+1}AX_n$, where M is an early transition metal, A is an A-group element of the periodic table, X corresponds to C and/or N, and *n* is typically 1, 2, or 3 [1]. They have attracted a strong interest because of their unique combination of properties, bridging the gap between metals and ceramics [2]. Whilst more than 80 different MAX phases have been discovered to date, MAX phases that contain aluminium as "A" element are of particular interest for high temperature applications, since these Al-based MAX phases form under oxidizing atmosphere at high temperature, typically > 1273 K, an external, cohesive and dense α-Al_2O_3 layer that protects the material against further oxidation [3][4].

Among all the Al-based MAX phases, Ti_2AlC, Ti_3AlC_2, and Cr_2AlC appear to possess the best oxidation and corrosion resistances [3], and so these MAX phases are excellent candidates to be operated at high temperature under aggressive environments due to the above mentioned response and the combination of other characteristic features of MAX phases, such as lightweight, high elastic modulus, thermal and electrical conductivity, good machinability with excellent thermal shock resistance and damage tolerance [5][6][7][8].

Whilst the excellent properties of MAX phases have triggered the development of various structures such as thin films and composites [9][10], porous MAX phases have been investigated to a minor extent despite their high potentials for various applications such as catalyst supports and heat exchangers. In fact, a number of main drawbacks of reticular ceramic structures, i.e., high brittleness, hard machining, complex joining with metals, and high coefficient of thermal expansion mismatch, could be overcome by using MAX phase foams. Most of the studies on MAX phase foams published to date are mainly focused on processing routes [11][12][13][14][15]. Different routes lead to tailor diverse final microstructures, such as porosity, pore size, and thickness of struts. Recently, Cr_2AlC foams have been produced by a sacrificial template and replica method [16][17].

The oxidation kinetics of Cr_2AlC was also investigated in a number of studies, and its excellent oxidation resistance was demonstrated [3][18][19][20][21].The oxidation starts at a temperature of ~ 1073K and leads to a dense and cohesive Al_2O_3 layer on the outer surface of Cr_2AlC owing to the outward diffusion of Al, beneath which porous Cr_7C_3 is formed. Effects of various factors such as cyclic oxidation and grain size on the oxidation were reported [5][22][23]. Also, a crack self-healing effect in Cr_2AlC due to the oxide scale formation was confirmed [24][25]. Most of the studies suggested that the oxidation kinetics of Cr_2AlC could be parabolic, whereas it has also been claimed that the oxidation kinetics of Cr_2AlC could be more complex, not expressed by a simple parabolic or cubic model [3]. The oxidation of porous Cr_2AlC has been also reported, which also confirmed remarkable formations of Al_2O_3 and Cr_7C_3 above 1073 K. It should be noted that Cr_2AlC is the only Al-based MAX phase which forms a carbide layer (Cr_7C_3) beneath Al_2O_3 layer after oxidation; however, the formation of Cr_7C_3 is quite problematic, because it could be easily oxidised in case of a breakage of Al_2O_3 layer, which will be catastrophic [3].

Compared to those studies on processing and oxidation of Cr_2AlC, the number of studies in literature on the mechanical properties is quite limited [24-30]. Mechanical properties of Cr_2AlC such as Young's modulus, flexural strength, and fracture toughness were studied mostly at room temperature [29-31]. Young's modulus and compressive strength at room temperature are found to be 288 GPa and 1159 MPa [28], respectively, which are comparable to other Al-based MAX phases such as Ti_3AlC_2 and Nb_2AlC [7]. Effects of various factors, such as impurity [30] and thermal shock [31], on the mechanical properties were investigated, whilst elastic properties determined by ab-initio molecular dynamics simulation were compared to the experimental values [29]. The temperature dependence of mechanical behaviour was also investigated on the basis of four-point bending tests, which revealed that the brittle-to-plastic transition occurs between 1073 K and 1273 K [32], close to that of the other Al-containing MAX phases, i.e., Ti_2AlC [33] and T_3AlC_2 [34].

The number of studies on mechanical properties of Cr_2AlC foam is even more limited. Recently, the compressive strength of Cr_2AlC foam was investigated in a uniaxial compression test at room temperature, which demonstrated that a pre-oxidation of Cr_2AlC foam at 1473 K for 1 h can significantly improve the compressive strength [16]. The effect of porosity on creep deformation behaviour of Cr_2AlC foam was investigated at elevated temperatures [26], which also revealed that the pre-oxidation can improve the creep resistance of Cr_2AlC foam by a few orders of magnitude. Both of the studies on the mechanical responses of Cr_2AlC foam have attributed the observed reinforcements to the oxide scales formed on the surface by the pre-oxidation; however, the oxidation kinetics and reinforcement mechanisms of Cr_2AlC foam are not well understood yet.

The aim of the current work is to investigate the oxidation mechanism and mechanical behaviour of Cr_2AlC foam. Cr_2AlC foam containing 53 vol.% porosity was oxidised at temperatures between 1173 K and 1473 K for times between 0 and 100 h, and the respective microstructure was examined. Uniaxial compression tests were performed at 298 K, 1273 K, and 1398 K using Cr_2AlC foams pre-oxidised at 1473 K for times between 0 and 50 h to examine mechanical properties, i.e., compressive strength and Young's modulus. On the basis of the results, the oxidation and fracture mechanisms of Cr_2AlC are elucidated, and a safety criterion for application is suggested.

2. Experimental

Processing of porous Cr_2AlC was carried out in two consecutives steps. First, Cr_2AlC powder was synthesized from its elemental constituents by liquid/solid state reaction, followed by a second step to consolidate porous samples at high temperature as reported with more details in [26][16]. Briefly, Cr, Al, and C powders (all from Alfa Aesar, Germany) were mixed in a molar ratio of 2:1.1:1, respectively, and uniaxially pressed at 100 MPa. Pellets were heated at 1673 K in argon atmosphere for 3 h to synthesize the Cr_2AlC phase. Then, Cr_2AlC samples were ground and milled to obtain the final powder with a unimodal particle size distribution and a mean particle size of 9 μm. Porous samples were produced by a sacrificial

template method, using ammonium hydrogen bicarbonate (NH_4HCO_3) as temporary space holder material. Cr_2AlC powder was mixed with 60 vol.% of NH_4HCO_3, followed by cold uniaxial pressing to obtain pellets of 13 mm diameter and 10 mm height. The space holders were burned-out at low temperature (353 K) in air, and the porous structures were consolidated at 1523 K for 5 h in argon atmosphere. The consolidated porous samples possessed a final porosity of 53 vol.% with pore sizes between 180 and 250 μm. The microstructure of the prepared sample is reported in detail in a previous study [18].

The prepared porous Cr_2AlC was cut into rectangular bar samples with dimensions of approximately 2.5×2.5×6 mm^3 using a diamond wheel saw. The bar samples were annealed at 1273 to 1473 K for 1 to 100 h in ambient air using an electric furnace. (Note that the oxidation at 1173 K and lower was too slow for the present evaluation.) The cross-section of the annealed samples was polished with abrasive papers (#2000) and investigated using a scanning electron microscope (SEM) and energy dispersion X-ray analysis (EDX) (TM3030, Hitachi High-Technologies) to examine the microstructure.

Then, the mechanical behaviours of porous Cr_2AlC annealed at 1473 K for different times were examined via uniaxial compression tests using a universal testing machine (AGS-X, Shimadzu) with an infrared furnace (IR-TP1-2, Yonekura). The testing temperatures were 298, 1273, and 1398 K with heating rates of 25–100 K/min. Each individual specimen was heated to the test temperature under a small pre-load of 0–5 MPa, followed by a holding period (20 min), and then the compressive stress was applied to the sample with the loading rate of 0.5 MPa/s. The specimen was rapidly cooled down after the test. All the test process (from the start of heating to the end of cooling) was finished within 30 min to avoid further oxidation for subsequent observation of fracture surfaces. The strain was measured using strain gauges (FLA, Tokyo Sokki) at room temperature, whilst only the displacement of the loading head was recorded at high temperatures. The obtained mechanical properties, i.e., compressive strength at each temperature and Young's modulus only at 298 K, are discussed especially their relationship to variations in microstructure.

3. Results

3.1 Microstructure of oxidised porous Cr_2AlC

Figure 1 shows the SEM images of polished cross-sections of porous Cr_2AlC specimens annealed at 1473 K for 3 h, 10 h, and 50 h (general views in (a)–(c) and at higher magnifications in (d)–(f)), respectively, where the material compositions shown here are assigned by the additional EDX analysis. The formation and growth of Al_2O_3 with porous Cr_7C_3 layers beneath are clearly observable (Fig. 1(a) and (d)), as similarly reported for dense Cr_2AlC in the previous studies [3][19]. The thickness of Al_2O_3 layer on the surface increases with annealing time, whilst the Cr_7C_3 layer beneath the Al_2O_3 grows thicker with a higher apparent rate and simultaneously becomes very porous (Fig. 1(b)). Accompanied by the formation of Al_2O_3 and Cr_7C_3, the remaining volume of porous Cr_2AlC matrix decreases with the annealing time. In addition to Cr_7C_3, Cr_2O_3 starts to appear in the sample annealed for 10 h (Fig. 1(b) and (e)), which grows then further with the annealing time up to 50 h, whilst some Al_2O_3 domains start to appear not only on the surface but also inside of the samples (Fig. 1(c)). In addition, the outer surface of Al_2O_3 becomes slightly porous after longer annealing (Fig. 1(f)), as similarly reported for dense Cr_2AlC [24]. The sample annealed for 50 h at 1473 K consists predominantly of Al_2O_3, Cr_7C_3, and Cr_2O_3, whilst there is only a small amount of remaining Cr_2AlC matrix.

Figure 2 summarises the thickness of Al_2O_3 layer Δh formed on the porous Cr_2AlC annealed at different temperatures in the range 1273 K to 1473 K for times between 0 and 100 h, where the Al_2O_3 thickness was determined on the basis of three SEM images with five different measuring points each. The Al_2O_3 layer becomes thicker for the samples annealed at higher temperature for longer annealing times, which agrees with the observations for dense Cr_2AlC [36]. The specimens with the same Al_2O_3 thickness have similar microstructures regardless of annealing condition. (It should be noted that the thickness of Cr_7C_3 layer was too varied all over the specimen to determine its average thickness, unlike Al_2O_3.)

3.2 Mechanical properties of oxidised porous Cr_2AlC

Figure 3(a) presents the stress vs strain relationships of porous Cr_2AlC pre-annealed at 1473 K for different times, obtained via uniaxial compression tests at 298 K. The relationships are mostly linear, and

all the specimens fractured in a brittle manner. Figure 3(b) and 3(c) present the stress vs displacement relationships obtained via the uniaxial tests at 1273 K and 1398 K, respectively. Some specimens tested at 1273 K, especially the ones annealed for short times at 1473 K, and all the specimens tested at 1398 K revealed a large plastic deformation before fracture or collapse. During the plastic deformation, the stress vs displacement curves displayed a number of small spikes, especially for the samples annealed for shorter times or tested at higher temperature (1398 K).

Figure 4 summarises the compressive strength of porous Cr_2AlC annealed at 1473 K for different hours in relation to Al_2O_3 thickness, where the compressive strength was evaluated using the maximum stress before large plastic deformations occurred. (Note that the thickness of Al_2O_3 layer formed on the specimens tested at high temperatures was re-evaluated using specimens separately annealed under the same conditions in order to take into account a growth of Al_2O_3 layer during the compression test, although its growth was quite small). The compressive strength at 298 K shows a significant increase from 76 MPa to 153 MPa when the Al_2O_3 thickness increased from 0 to ~ 2.5 μm, followed by a gradual decrease to 50 MPa with increase of the Al_2O_3 thickness to 7.6 μm. At 1273 K, the compressive strength of porous Cr_2AlC (without pre-oxidation) is considerably lower than the strength at 298 K, and the Al_2O_3 layer of 3 μm does not yet reinforce the porous Cr_2AlC unlike at 298 K. However, the strength shows a noticeable increase reaching a maximum of 138 MPa for an Al_2O_3 thickness of 4.9 μm, followed by a slight decrease to 110 MPa with increase of the Al_2O_3 thickness to 8.1 μm. The strength at 1398 K exhibits a similar trend to that at 1273 K, whilst the variation is smaller, and its maximum is 128 MPa for a 4.5 μm Al_2O_3 layer. (It may appear to increase monotonically except for the one annealed for 6 h.)

Figure 5(a) summarises the Young' modulus of porous Cr_2AlC annealed at 1473 K for different times in relation to the Al_2O_3 thickness, obtained via compression tests at 298 K. The modulus shows a very similar trend as the compressive strength presented in Fig. 4(a), although its variation is much smaller than that of the strength. Figure 5(b) presents the Young's modulus vs compressive strength at 298 K. There appears to be a good correlation between the Young's modulus and compressive strength, whilst the fracture strain ε_f also correlates with the strength, where ε_f was determined using the strain corresponding to the maximum

stress.

Figure 6 presents the SEM images of fractured surface of oxidised porous Cr_2AlC annealed for 0, 3, and 20 h, respectively, fractured at 298 K ((a)-(c)) and 1273 K ((d)-(f)). The predominant fracture mode of porous Cr_2AlC is intergranular in all cases. There are very small Al_2O_3 particles observable on the surface of intergranularly-fractured grains, as reported in literature [28], which exist already in the original material as can be seen in Fig. 1(d) as small dots. Some delaminations in the grains are also visible in the transgranularly-fractured grains, which are found in the vicinity of the Al_2O_3 layers/domains. The cracks appear to propagate along the grain boundaries in the Cr_2AlC matrix and also connecting pores (internally covered with Al_2O_3) in Cr_2AlC and Cr_7C_3. There are more transgranular fractures with rougher surfaces when fractured at high temperatures, especially for less-oxidised samples. No significant deformation of grains is observed. On the fracture surface of Al_2O_3, the columnar (inner) and equiaxial (outer) structures are confirmed, as reported for dense Cr_2AlC similarly [24]. Few delaminations of the Al_2O_3 layer were observed after the fracture tests at any temperatures.

4. Discussion

4.1 Oxidation process of porous Cr_2AlC

Figure 7 illustrates schematically the oxidation process of porous Cr_2AlC, which is suggested on the basis of the SEM observations shown in Figs. 1 and 6. On the surface the as-prepared Cr_2AlC matrix (e.g. area A in Fig. 7(a)), has no oxidation layers at the beginning (Fig. 7(b)). As annealed, a dense and continuous Al_2O_3 layer grows on the surfaces including pore surfaces, beneath which porous Cr_7C_3 forms (Fig. 7(c)). As the Al_2O_3 layer thickens, also the Cr_7C_3 gets thicker and more porous with a higher rate (Fig. 7(d, e)). In the thin struts (e.g. area B in Fig. 7(a)), the oxidation proceeds in a similar way but with a faster rate of Cr_2AlC consumption due to higher specific surface area, which results in the breakage of Al_2O_3 layers probably caused by a large volumetric expansion of porous Cr_7C_3 (Fig. 7(d')), as can be observed in Fig. 1(e). The breakage of Al_2O_3 layers leads to an oxygen inflow, which oxidises the Cr_7C_3 into Cr_2O_3, followed by the spallation of Cr_2O_3 and the formation of discontinuous Al_2O_3 barriers/domains inside the

material (see Fig. 7(e')). At the end, the material consists mainly of Al_2O_3, Cr_7C_3, and Cr_2O_3 (Fig. 7(e)), where only a small amount of Cr_2AlC remains. For instance, the porous Cr_2AlC annealed at 1473 K for 3 h, 10 h, and 50 h has the microstructures illustrated in Fig. 7(c), (d, d'), and (e, e'), respectively. (This suggested mechanism appears to be representative when oxidised in the present temperature range, i.e., 1273 K to 1473 K, but not applicable to oxidation taking place at 1723 K or higher due to incongruent melting [1].)

The thickness of Al_2O_3 layer increases monotonically with the annealing time and temperature as presented in Fig. 2. The microstructures with the same Al_2O_3 thickness are similar to each other regardless of the annealing condition, which indicates that the development of the Al_2O_3 layer might be represented by its thickness. The relationship between the time t and the Al_2O_3 thickness Δh at each temperature can be approximated by a parabolic law [3], $\rho\Delta h = (k_p t)^{1/2}$, as shown in Fig. 8(a), where ρ is density of Al_2O_3 (3.9×10^3 kg/m^3 [35]) and k_p is an oxidation constant. Figure 8(b) is the Arrhenius plot of the oxidation constant, where k_p appears to follow a thermally-activated process. (Note here that the data of samples annealed at 1473 K for longer than 20 h are excluded due to the excessive oxidation.) The obtained activation energy for the Al_2O_3 formation of porous Cr_2AlC was 346 kJ/mol, which is comparable to the one obtained for powder Cr_2AlC using thermogravimetric analysis (297 kJ/mol) [34]. The increase of the Al_2O_3 thickness Δh with annealing time measured at ambient temperature can thus be expressed by the following relationship:

$$\rho\Delta h = \{16677\, t \exp(-41632/T)\}^{1/2} \quad [\mathrm{kg/m^2}] \qquad (1),$$

where the coefficient of determination R^2 = 0.9998 for Eq. (1) and R^2 = 0.936–0.996 for the original parabolic curve fittings (Fig. 8). (The relatively low R^2 values could be mostly attributed to the large variations of the measured thickness shown in Fig. 2.) It should be noted that, if a cubic law $\rho\Delta h = (k_p t)^{1/3}$ is applied, the following relationship results:

$$\rho\Delta h = \{2.66\times10^6\, t \exp(-54423/T)\}^{1/3} \quad [\mathrm{kg/m^2}] \qquad (2),$$

where R^2=0.9955 for Eq. (2) and R^2= 0.932–0.986 for original cubic curve fittings. These results suggest that the parabolic law appears to provide a better fitting than the cubic law in the present case, although the

exact oxidation kinetics of Cr_2AlC is considered to be more complex compared to other Al-based MAX phases and not to follow simple parabolic or cubic law [3].

4.2. Mechanical Properties of oxidised porous Cr_2AlC

4.2.1. Room Temperature

As shown in Figs. 4 and 5, the compressive strength and Young's modulus at 298 K have their maximum values (150 MPa and 63 GPa, respectively) for a thin Al_2O_3 layer (c.a. 2.5 μm). However, further growth of the Al_2O_3 layer (up to 8 μm) rather deteriorates the improvements. It can be considered that the continuous and cohesive Al_2O_3 layer formed on Cr_2AlC via porous Cr_7C_3 plays an important role in the improvement of the mechanical properties, as has been seen for the high-temperature creep resistance reported in the previous study [26].

Figure 9 illustrates the fracture modes of the oxidised porous Cr_2AlC with crack propagation paths, which are derived on the basis of the SEM observations of cross-sections and fracture surfaces. As a general rule, the predominant fracture mode of porous Cr_2AlC is intergranular as verified for the dense Cr_2AlC [32], whilst a transgranular fracture is additionally observed in grains that are constrained by the Al_2O_3 layers/domains or material boundaries (Fig. 9(a)). Non-oxidised porous Cr_2AlC fractures intergranualarly, possibly starting from defects such as very small Al_2O_3 particles at grain boundaries. Slightly-oxidised one fractures in the same way, where the crack propagation starting from the grain boundaries of Cr_2AlC could be hindered by the Al_2O_3 layer (Fig. 9(b)), resulting in the reinforcement of the material. If annealed longer, the Cr_7C_3 layers becomes more porous with larger pore sizes, where the inner surface of pores is also oxidised, where the cracks appear to initiate from / propagate through these pores due to stress concentrations (Fig. 9(c)) [22]. An excessive oxidation causes the breakages of Al_2O_3, followed by a material decomposition as explained in Fig. 7, which seems to result in a weakening of the mechanical properties due to multiple possible crack paths, i.e., (Fig. 9(d)). Cracks connecting the pores are frequently observed in the vicinity of material boundaries (i.e. Cr_2O_3/Cr_7C_3 and Cr_7O_3/Cr_2AlC). Therefore, a slight oxidation can improve the mechanical properties, especially the strength, due to the dense and

cohesive Al_2O_3 layer preventing the crack to propagate from inside; however, an excessive oxidation causes the breakage of Al_2O_3, followed by the decomposition of Cr_2AlC, which deteriorates the strength improvements.

For further discussion, the variation of mechanical properties was estimated by a simple theoretical model: The properties of porous Cr_2AlC with Al_2O_3 and Cr_7C_3 layers might be roughly expressed by a Voigt model, $X=\Sigma X_i \phi_i$ ($_i$ = 1~3) [37], where X_i is property (Young's modulus E or compressive strength σ_c) of each phase, ϕ_i is volume fraction (= V_i/V, where V_i is volume of each phase and V is the total volume), and i is material index (1 = porous Cr_2AlC, 2 = dense Al_2O_3, 3 = porous Cr_7C_3, hereafter). The Voigt model was chosen in this study, as this is one of the simplest models which can predict reinforcements. For the Al_2O_3 phase (i = 2), Young's modulus and compressive strength are 340 GPa and 2500 MPa [35], respectively, and the variation of volume fraction was estimated based on Eq. (1) assuming an average pore size of 215 μm [16]. For the porous Cr_2AlC phase (i = 1), the apparent volume including pores is assumed to be constant, whereas its porosity is considered to increase if annealed (considering a volume decrease in the microstructure) following a chemical reaction (i.e., the formation of 1 mol of Al_2O_3 costing 2 mol of Cr_2AlC). The variation of mechanical properties of Cr_2AlC with increasing porosity at 298 K is estimated on the basis of preliminary experimental results shown in Fig. 10. (The modulus and strength were obtained in identical compressive tests using specimens with the porosity of 2%, 53%, and 75%. Details on the used materials can be found in our previous studies [26][27].) For porous Cr_7C_3 (i = 3), the apparent volume (including pores) is roughly assumed to increase four times larger than the volume of Al_2O_3, which leads to a total volume expansion that agrees with the one experimentally observed, whilst its mechanical properties are to be variables. Table 1 summarises the properties used for the estimations.

Figure 11 presents the variation of mechanical properties as estimated by the Voigt model with Cr_7C_3 properties (X_3) as variables. (Here, the properties of oxidised porous Cr_2AlC with A_2O_3 thicker than 5.5 μm are not discussed since the microstructure is different due to the excessive oxidation.) In the early oxidation stage, i.e., when the Al_2O_3 thickness $\Delta h \leq 3$ μm, the increase of total Young's modulus E can be explained

well by the reinforcement of Al_2O_3 layer as shown in Fig. 11(a), where the porous Cr_7C_3 (E_3 = 165 GPa) is not yet dominant in the structure. If annealed longer, i.e., when $\Delta h \geq 3$ μm, more porous Cr_7C_3 with lower modulus (E_3 = 65~110 GPa) forms and becomes more dominant in the structure, which appears to result in a decrease of the total modulus. The compressive strength shown in Fig. 11(b) is significantly enhanced by the Al_2O_3 layer, as the strength of Al_2O_3 is much higher than porous Cr_2AlC. For Δh = 3 μm, the maximum strength of 153 MPa can be modelled using the σ_{c3} = 280 MPa. For $\Delta h \geq 3$ μm, where porous Cr_7C_3 becomes dominant, the decreasing of σ_{c3} (e.g. σ_{c3} as low as 10 MPa) does not predict the decrease of the total strength unlike E, because the strength Al_2O_3 is much higher than that of the others. This suggests that the decrease of total strength for $\Delta h \geq 3$ μm might be attributed to the breakage of the continuous Al_2O_3 layers.

Therefore, the moderate variation of modulus in relation to Al_2O_3 thickness is attributed to the combination of volume fractions of Al_2O_3 and porous Cr_7C_3, whereas the considerable variation of strength can be attributed to the continuity of the cohesive Al_2O_3 layer. Although the present property estimations contain various assumptions due to a number of uncertain parameters, it is helpful to understand the variation of mechanical properties with respect to oxidation.

4.2.2. High Temperature

A mechanical behaviour with plasticity was observed at 1273 K only for less-oxidised specimens and at 1398 K for all the specimens. The porous Cr_2AlC specimens that did not show a large plastic deformation fracture in a brittle manner, whereas the plastically-deformed ones tend to collapse. The porous Cr_2AlC teste at high temperatures has more intergranular fracture with rougher fracture surfaces, compared to the ones tested at 298 K. Transgranular fracture with delaminations in the grains appears mostly just beneath the Al_2O_3. The rough surface, especially found for less-oxidised specimens, can be attributed to dimples caused by a plastic deformation around very small Al_2O_3 particles at grain boundaries, as illustrated in Fig. 9(e), which could lead to the macroscopically-observed plastic deformation shown in Fig. 3. (It is worth noting that this result implies that less segregation of Al_2O_3 at the grain boundaries would suppress the

plastic deformation at high temperatures, leading to an increase of the brittle-plastic transition temperature, which requires however further verification.) In addition, the small spikes observed in Fig. 3, which are found only during the plastic deformation at high temperature, might be related to further oxidation probably followed by the breakage of the oxidation layer during the deformation, as less annealed samples at higher temperatures show these spikes more frequently.

As shown in Fig. 4, the sample annealed at 1473 K for 3 h (with Δh = 2.5 μm) has significantly improved mechanical properties when measured at 298 K, whereas prominent but smaller improvements are observed with thicker Al_2O_3 (Δh = c.a. 5 μm) at 1273 K and 1398 K. To understand this apparent difference between the behaviour at room and high temperatures, additional compression tests were performed in the temperature range from 298 K to 1398 K, in particular around 1273 K, only for porous Cr_2AlC annealed at 1473 K for 3 h (Δh = c.a. 2.5 μm). Figure 12 shows the compressive strength of porous Cr_2AlC annealed at 1473 K for 3 h as a function of temperature, where the strength of porous Cr_2AlC annealed at 1473 K for 0, 10, and 50 h are shown for comparison. (Note that the small growth of the Al_2O_3 layer during the test is not considered here.) The improved strength is retained from 298 K to 1248 K (with only a 10% of variation), where all the samples fracture in a brittle manner, whereas it drops sharply around 1273 K, followed by a slight recovery at 1398 K. For dense Cr_2AlC, mechanical behaviour with obvious plasticity was observed above 1173 K in a four-point bending test [32], accompanied by an abrupt decrease of the flexural strength. It was concluded that the brittle-to-plastic transition temperature was between 1173 and 1273 K [32]. Therefore, although the mechanical properties of the porous Cr_2AlC matrix without oxidation should decrease above the temperature of 1173 K, the pre-formed Al_2O_3 (Δh = 2.5 μm) leads to a retained strength of the porous Cr_2AlC up to 1273 K. However, when the strength of Cr_2AlC matrix becomes too low above 1173 K, it requires a thicker Al_2O_3 layer (Δh = 5 μm) to retain a superior strength. At high temperatures, the decomposition of the material does not degrade the strength much, probably because the amount of Al_2O_3 with its superior properties plays an important role.

4.3. Recommended lifetime

On the basis of the present experimental results, a safety criterion of porous Cr_2AlC for application at elevated temperature is discussed in the following from a mechanical point of view.

When as-prepared (i.e., non-oxidised) porous Cr_2AlC is used at elevated temperature, it will be gradually oxidised. It was observed that some oxidation can monotonically improve the mechanical properties of porous Cr_2AlC, whereas an excessive oxidation could ruin the improvement. The variation of mechanical properties during oxidation (at 1473 K and lower) can be attributed to the microstructural changes illustrated in Figs. 7 and 8, which can be represented by the Al_2O_3 thickness determined by Eq. (1). For instance, at operation temperature 1273 K, the initial compressive strength of porous Cr_2AlC (almost) without oxidation is about 58 MPa (as shown in Fig. 4(b)), and it is expected to monotonically increase during usage at 1273 K until the thickness of the Al_2O_3 layer reaches ~ 5 μm, which can be obtained after ~1008 h according to Eq. (1). In other words, as-prepared porous Cr_2AlC can be used without property degradation (rather with some property improvement) until 1008 h at 1273 K. Below 1243 K, the mechanical property will be retained or even improved until the Al_2O_3 layer grows to ~2.5 μm, assuming that mechanical properties remain unchanged in the temperature range from 298 K to 1243 K, as shown in Fig. 12.

Figure 13 summarises the recommended maximum operation times t_{app} without mechanical property degradation at operation temperatures from 1100 K to 1400 K, which can be determined by

$$t_{app} = (\rho \Delta h_x)^2 \exp(41632 / T) / 16677 \quad [s] \tag{3},$$

where Δh_x is the thickness of Al_2O_3 where the mechanical properties (i.e., here compressive strength) show their maxima, which is assumed to be 2.5 μm for $T \leq 1273$ K and 5 μm for $T \geq 1273$ K, respectively. It should be noted that the material would deform plastically at temperatures above 1173 K.

5. Conclusion

Oxidation kinetics and mechanical behaviour of Cr_2AlC were investigated in this study. The porous Cr_2AlC with a porosity of 53% was oxidised at different temperature, and the microstructures of the

oxidised porous Cr_2AlC specimens were examined. Uniaxial compression tests were performed at various tempertures using porous Cr_2AlC oxidised at 1473 K to characterize the mechanical properties.

Overall the oxidation of porous Cr_2AlC is similar to the oxidation of its dense counterpart: A continuous and cohesive Al_2O_3 layer forms on the Cr_2AlC matrix, beneath which porous Cr_7C_3 forms. The oxidation mechanism can be roughly expressed by a parabolic law. However, an excessive oxidation takes place, first in thin struts, where the formed Al_2O_3 layer breaks, followed by an oxygen inflow and decomposition of the inner material. This excessive oxidation in thin struts appears to start when the thickness of the Al_2O_3 layer exceeds 2.5 μm.

At room temperature (298 K), non-oxidised porous Cr_2AlC fractures intergranularly, possibly with crack initiations from very small Al_2O_3 particles at grain boundaries. Constrained grains tend to fracture transgranularly with delaminations. Slight oxidation significantly improves the mechanical properties, especially the compressive strength, as the Al_2O_3 layer formed on the surface can prevent the initiated cracks to propagate from inside outward. However, an excessive oxidation (with the Al_2O_3 layer thicker than 2.5 μm) deteriorates the improvement in the strength, which can be explained by a breakage of the Al_2O_3 layer at thin struts followed by a material decomposition.

At elevated temperatures (1273 K and 1398 K), non-oxidised porous Cr_2AlC fractures intergranularly accompanied with a plastic deformation around very small Al_2O_3 particles at grain boundaries, which results in a macroscopic plastic deformation. Although the predominant fracture mode of slightly-oxidised porous Cr_2AlC is also intergranular, a thicker Al_2O_3 layer (~5 μm) is required to reinforce the material, since the Cr_2AlC matrix softens and gets weaker at high temperatures. The brittle-to-plastic transition temperature appears to be slightly raised by the Al_2O_3 layer with a thickness of 2.5 μm from 1173 to 1273 K for non-oxidised, dense Cr_2AlC.

Lastly, a safety criterion, i.e., a maximum operating time at high temperature, is suggested on the basis of the oxidation and fracture mechanisms discussed above: for example, the non-oxidised porous Cr_2AlC can be used at 1273 K for up to 1008 h with no property degradation but rather with some improvement.

ACKNOWLEDGEMENTS

This work is supported by a Bilateral Program between the Japan Society for the Promotion of Science and the German Academic Exchange Service (JSPS/DAAD) with the project number JPJSBP120193505 for JSPS, 57457777 for DAAD, respectively. Jesus Gonzalez-Julian thanks the financial support by the Germany's Federal Ministry of Education and Research ("Bundesministerium für Bildung und Forschung") under the MAXCOM project (03SF0534).

References

[1] M.W. Barsoum, MAX Phases. Properties of machinable rernary carbides and nitrides, Wiley VCH, 2013.

[2] B.M. Radovic, M.W. Barsoum, MAX phases : Bridging the gap between metals and ceramics, Am. Ceram. Soc. Bull. 92 (2013) 20–27.

[3] D.J. Tallman, B. Anasori, M.W. Barsoum, A critical review of the oxidation of Ti_2AlC, Ti_3AlC_2 and Cr_2AlC in air, Mater. Res. Lett. 1 (2013) 115–125.

[4] J.L. Smialek, Oxygen diffusivity in alumina scales grown on Al-MAX phases, Corros. Sci. 91 (2015) 281–286.

[5] J. Gonzalez-Julian, T. Go, D.E. Mack, R. Vaßen, Environmental resistance of Cr_2AlC MAX phase under thermal gradient loading using a burner rig, J. Am. Ceram. Soc. 101 (2018) 1841–1846.

[6] J.L. Smialek, Environmental resistance of a Ti_2AlC-type MAX phase in a high pressure burner rig, J. Eur. Ceram. Soc. 37 (2017) 23–34..

[7] M.W. Barsoum, M. Radovic, Elastic and mechanical properties of the MAX phases, Annu. Rev. Mater. Res. 41 (2011) 195–227.

[8] Z. Wang, J. Sund, B. Xua, Y. Liua, P. Kea, A. Wang, Reducing the self-healing temperature of Ti_2AlC MAX phase coating by substituting Al with Sn, J. Eur. Ceram. Soc. 40 (2020) 197–201.

[9] P. Eklund, M. Beckers, U. Jansson, H. Högberg, L. Hultman, The $M_{n+1}AX_n$ phases: Materials science and thin-film processing, Thin Solid Films. 518 (2010) 1851–1878.

[10] J. Gonzalez-Julian, J. Llorente, M. Bram, M. Belmonte, O. Guillon, Novel Cr_2AlC MAX-phase/SiC fiber composites: Synthesis, processing and tribological response, J. Eur. Ceram. Soc. 37 (2017).

[11] M. Potoczek, E. Guzi de Moraes, P. Colombo, Ti_2AlC foams produced by gel-casting, J. Eur. Ceram. Soc. 35 (2015) 2445–2452.

[12] T. Fey, M. Stumpf, A. Chmielarz, P. Colombo, P. Greil, M. Potoczek, Microstructure, thermal conductivity and simulation of elastic modulus of MAX-phase (Ti_2AlC) gel-cast foams, J. Eur. Ceram. Soc. 38 (2018) 3424–3432.

[13] B. Velasco, E. Gordo, L. Hu, M. Radovic, S.A. Tsipas, Influence of porosity on elastic properties of Ti_2AlC and Ti_3SiC_2MAX phase foams, J. Alloys Compd. 764 (2018) 24–35.

[14] B. Velasco, E. Gordo, S.A. Tsipas, MAX phase Ti2AlC foams using a leachable space-holder material, J. Alloys Compd. 646 (2015) 1036–1042.

[15] C.R. Bowen, T. Thomas, Macro-porous Ti2AlC MAX-phase ceramics by the foam replication method, Ceram. Int. 41 (2015) 12178–12185.

[16] J. Gonzalez-Julian, S. Onrubia, M. Bram, C. Broeckmann, R. Vaßen, O. Guillon, High temperature oxidation and compressive strength of Cr_2AlC MAX phase foams with controlled porosity, J. Am. Ceram. Soc. 101 (2018) 542–552.

[17] S. Karimi, T. Go, R. Vaßen, J. González-Julián, Cr_2AlC MAX phase foams by replica method, Mater. Lett. 240 (2019) 271-274.

[18] J.L. Smialek, S. Gray, Type II Hot corrosion screening tests of a Cr_2AlC MAX phase compound, Oxid. Met. 90 (2018) 555–570.

[19] J.L. Smialek, Oxidation of Al_2O_3 Scale-forming MAX phases in turbine environments, Metall. Mater. Trans. A Phys. Metall. Mater. Sci. (2017) 1–11.

[20] J.L. Smialek, J.A. Nesbitt, T.P. Gabb, A. Garg, R.A. Miller, Hot corrosion and low cycle fatigue of a Cr_2AlC-coated superalloy, Mater. Sci. Eng. A. 711 (2018) 119–129.

[21] Z. Wanga, G. Ma, L. Liu, L. Wang, P. Ke , Q. Xue, A. Wang, High-performance Cr_2AlC MAX phase coatings: Oxidation mechanisms in the 900–1100°C temperature range, Corrosion Sci. 167 (2020) 108492.

[22] D.B. Lee, T.D. Nguyen, J.H. Han, S.W. Park, Oxidation of Cr_2AlC at 1300 °C in air, Corros. Sci. 49 (2007) 3926–3934.

[23] S. Li, X. Chen, Y. Zhou, G. Song, Influence of grain size on high temperature oxidation behavior of Cr2AlC ceramics, Ceram. Int. 39 (2013) 2715–2721.

[24] H.J. Yang, Y.T. Pei, J.T.M. De Hosson, Oxide-scale growth on Cr_2AlC ceramic and its consequence for self-healing, Scr. Mater. 69 (2013) 203–206.

[25] A.S. Farle, C. Kwakernaak, S. van der Zwaag, W.G. Sloof, A conceptual study into the potential of Mn+1AXn-phase ceramics for self-healing of crack damage, J. Eur. Ceram. Soc. 35 (2015) 37–45.

[26] W. Araki, J. Gonzalez-Julian, J. Malzbender, High temperature compressive creep of dense and porous Cr_2AlC in air, J. Eur. Ceram. Soc. 39 (2019) 3660–3667.

[27] J. Gonzalez-Julian, S. Onrubia, M. Bram, O. Guillon, Effect of sintering method on the microstructure of pure Cr2AlC MAX phase ceramics, J. Ceram. Soc. Japan. 124 (2016) 415–420.

[28] W. Tian, P. Wang, G. Zhang, Y. Kan, and Y. Li, Mechanical properties of Cr_2AlC ceramics, J. Am. Ceram. Soc., 90 (2007) 1663–1666.

[29] J.M. Schneider, D.P. Sigumonrong, D. Music, C. Walter, J. Emmerlich, R. Iskandar and J. Mayer, Elastic properties of Cr_2AlC thin films probed by nanoindentation and ab initio molecular dynamics, Scripta Mater. 57 (2007) 1137–1140.

[30] G. Ying, X. He, M. Li, S. Du, W. Han, and F. He, Effect of Cr_7C_3 on the mechanical, thermal, and electrical properties of Cr_2AlC, J. Alloys Compd. 509 (2011) 8022– 8027.

[31] H. Li, S. Li, and Y. Zhou, Cyclic thermal shock behaviour of a Cr_2AlC ceramic, Mater. Sci. Eng. A 607 (2014) 525–529.

[32] W. Tian, Z. Sun, Y. Du, and H. Hashimoto, Mechanical properties of pulse discharge sintered Cr_2AlC at 25–1000 °C, Materials Letters 63 (2009) 670–672.

[33] H. Gao, R. Benitez, W. Son, R. Arroyave, and M. Radovic, Structural, physical and mechanical properties of $Ti_3(Al_{1-x}Ti_xSi_x)C_2$ solid solution with x=0–1, Mater. Sci. & Eng. A 676 (2016) 197–208.

[34] Y. Bai, X. He, C. Zhu, and G. Chen, Microstructures, electrical, thermal, and mechanical properties of bulk Ti_2AlC synthesized by self-propagating high-temperature combustion synthesis with pseudo hot isostatic pressing, J. Am. Ceram. Soc. 95 (2012) 358–364.

[35] Matweb, http://www.matweb.com/search/DataSheet, Overview–Alumina, 98%, Al_2O_3 (Mar 2020).

[36] Z.J. Lin, M.S. Li, J.Y. Wang, Y.C. Zhou, High-temperature oxidation and hot corrosion of Cr_2AlC, Acta Mater. 55 (2007) 6182–6191.

[37] W. Voigt, Ueber die Beziehung zwischen den beiden Elasticitätsconstanten isotroper Körper, Ann.

Phys. 274 (1889) 573–587.

Captions

Table 1 Parameters used for the property estimations in Fig. 11.

Figure 1 Cross-sectional SEM images of porous Cr_2AlC annealed 1473 K for different hours: (a) 3 h, (b) 10 h, and (c) 50 h at lower magnification, and (d) 3 h, (e) 10 h, and (f) 50 h at higher magnifications. Each area is assigned to Cr_7C_3, Cr_2AlC, Cr_2O_3, Al_2O_3, and pore (embedding resin), respectively, from the brightest colour.

Figure 2 Thickness of Al_2O_3 layer formed on porous Cr_2AlC annealed at different temperatures and times.

Figure 3 Mechanical behaviours of porous Cr_2AlC annealed at 1473 K for different hours, obtained in the uniaxial compression test at different temperatures: (a) 298 K, (b) 1273 K, and (c) 1398 K.

Figure 4 Compressive strength and Al_2O_3 thickness of porous Cr_2AlC annealed at 1473 K for different hours, obtained in the uniaxial compression test at different temperatures: (a) 298 K, (b) 1273 K, and (c) 1398 K. The symbol * represents the specimen annealed at 1373 K for 1 h. The symbols ○ and ● express predominant mechanical behaviours: ○ is for brittle fracture, whilst ● is for plastic deformation.

Figure 5 Young's modulus of porous Cr_2AlC annealed at 1473 K for different hours, obtained in the uniaxial compression tests at 298 K with relation to (a) Al_2O_3 thickness and (b) compressive strength at 298 K. The symbol * represents the specimen annealed at 1373 K for 1 h. The inset in (b) shows the strength vs the fracture strain relationship.

Figure 6 Fracture surface of porous Cr_2AlC annealed at 1473 K for different hours tested in the uniaxial compression at different temperatures: (a-c) and (d-f) are fractured at 298 K and 1273 K respectively,

whilst (a)(d), (b)(e), (c)(f) are annealed for 0, 3, and 20 h, respectively. The white and grey arrows indicate the cracks along grain boundaries and the delaminations in grains, respectively.

Figure 7 Oxidation mechanism of porous Cr_2AlC: (a) General view, (b)-(e) oxidation process on the surface of Cr_2AlC (e.g. area A in (a)), and (d')(e') oxidation process around thin strut (e.g. area B in (a), corresponding stage to (d) and (e)).

Figure 8 Al_2O_3 growth on porous Cr_2AlC oxidised under different conditions: (a) Approximations by the parabolic law and (b) Arrhenius plot of oxidation constant.

Figure 9 Fracture mode with crack propagation path in oxidised porous Cr_2AlC: (a) Al_2O_3 particles at the grain boundaries and transgranular fractures with delaminations (shown as striped patterns) in the constrained grains, (b) intergranular fracture in a slightly-oxidised sample, (c) in a more oxidised sample, (d) in an excessively-oxidised sample (corresponding to Fig. 7(e')), and (e) intergranular fracture with dimple formations at high temperatures. The dashed lines indicate possible crack propagation paths.

Figure 10 Mechanical properties of Cr_2AlC with different porosities obtained in the uniaxial compression test at 298 K and the approximations.

Figure 11 Predictions of mechanical properties of oxidised porous Cr2AlC at 298 K: (a) Young's modulus and (b) compressive strength.

Figure 12 Compressive strength of porous Cr_2AlC annealed at 1473 K for 3 h as a function of temperature from 298 K to 1398 K. The strength of porous Cr_2AlC annealed at 1473 K for 0, 10, and 50 h are shown for comparison. The open and filled symbols represent brittle fracture and plastic deformation, respectively.

Figure 13 Recommended operating condition with Al_2O_3 thickness. The optimum Al_2O_3 thickness is assumed to be 2.5 μm for the temperature $T \leq 1273$ K and 5 μm for $T \geq 1273$ K, respectively, whilst the BRT (the brittle-to-plastic transition temperature) is 1273 K for the Al_2O_3 thickness of 2.5 μm.

Table 1 Parameters used for the property estimations in Fig. 11.

Material	Index i	Porosity p	Volume V_i	Young's modulus E_i, GPa	Compressive strength σ_{ci}, MPa
Cr_2AlC	1	Porous ($\geq$ 53%)	Apparently constant	E_1= 340 exp(–3.62p) (Fig. 10)	σ_{c1}= 1370 exp(–5.46p) (Fig. 10)
Al_2O_3	2	Dense	Eq. (1)	340	2500
Cr_7C_3	3	Porous	Four times V_2	Variable	Variable

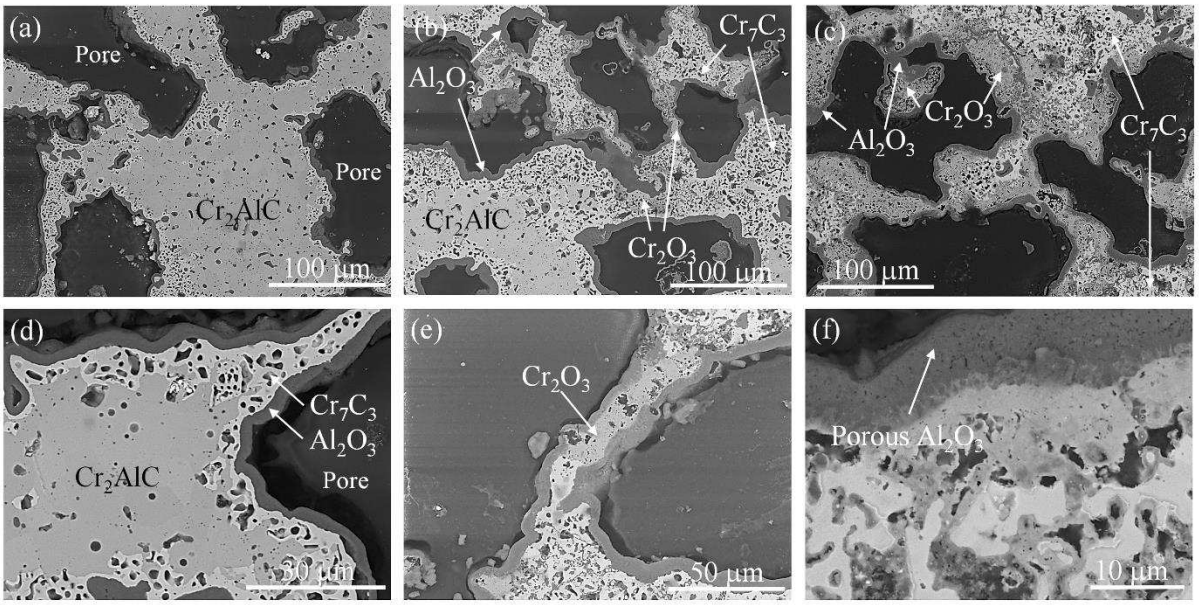

Figure 1 Cross-sectional SEM images of porous Cr_2AlC annealed 1473 K for different hours: (a) 3 h, (b) 10 h, and (c) 50 h at lower magnification, and (d) 3 h, (e) 10 h, and (f) 50 h at higher magnifications. Each area is assigned to Cr_7C_3, Cr_2AlC, Cr_2O_3, Al_2O_3, and pore (embedding resin), respectively, from the brightest colour.

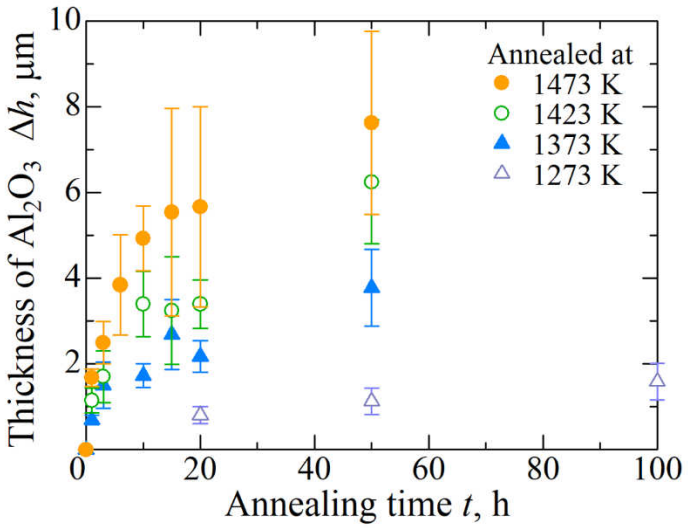

Figure 2 Thickness of Al_2O_3 layer formed on porous Cr_2AlC annealed at different temperatures and times.

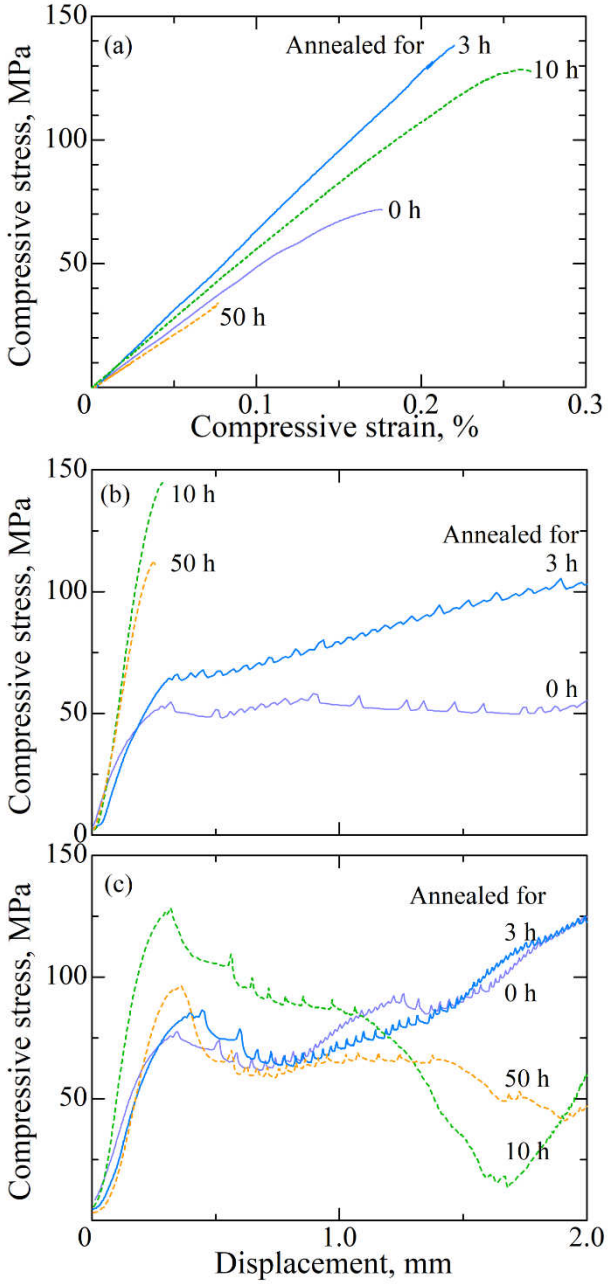

Figure 3 Mechanical behaviours of porous Cr_2AlC annealed at 1473 K for different hours, obtained in the uniaxial compression test at different temperatures: (a) 298 K, (b) 1273 K, and (c) 1398 K.

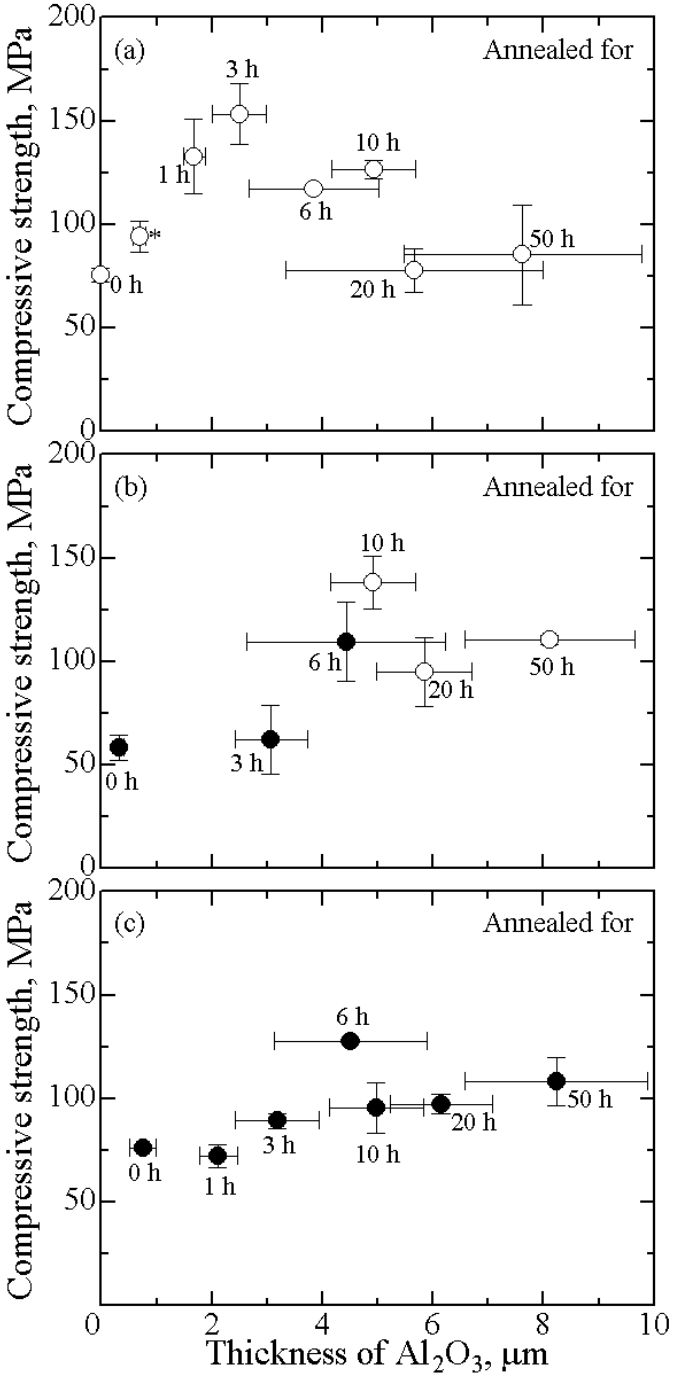

Figure 4 Compressive strength and Al_2O_3 thickness of porous Cr_2AlC annealed at 1473 K for different hours, obtained in the uniaxial compression test at different temperatures: (a) 298 K, (b) 1273 K, and (c) 1398 K. The symbol * represents the specimen annealed at 1373 K for 1 h. The symbols ○ and ● express predominant mechanical behaviours: ○ is for brittle fracture, whilst ● is for plastic deformation.

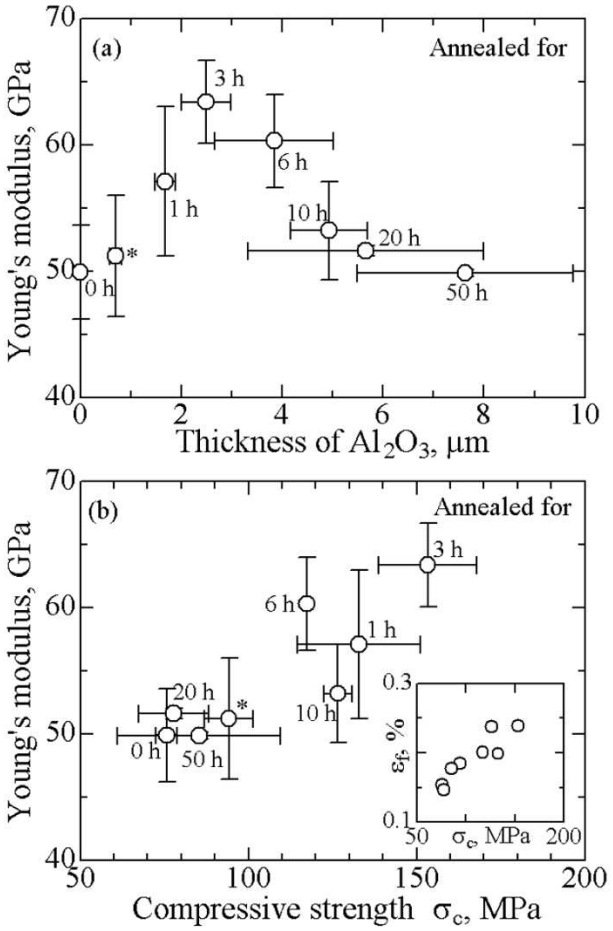

Figure 5 Young's modulus of porous Cr_2AlC annealed at 1473 K for different hours, obtained in the uniaxial compression tests at 298 K with relation to (a) Al_2O_3 thickness and (b) compressive strength at 298 K. The symbol * represents the specimen annealed at 1373 K for 1 h. The inset in (b) shows the strength vs the fracture strain relationship.

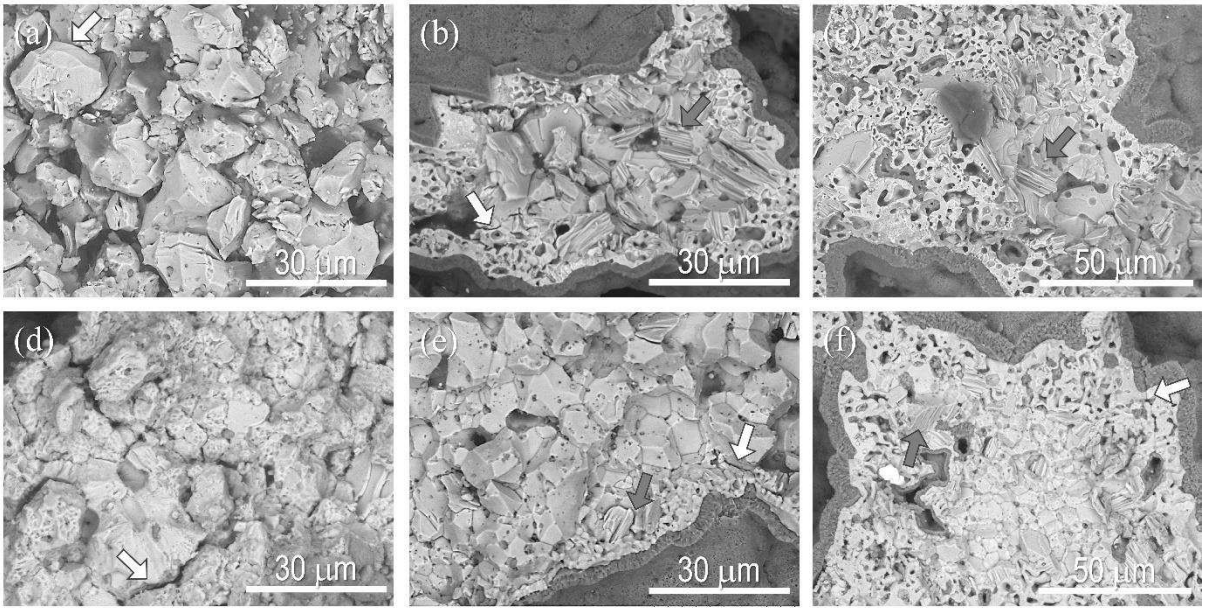

Figure 6 Fracture surface of porous Cr_2AlC annealed at 1473 K for different hours tested in the uniaxial compression at different temperatures: (a-c) and (d-f) are fractured at 298 K and 1273 K respectively, whilst (a)(d), (b)(e), (c)(f) are annealed for 0, 3, and 20 h, respectively. The white and grey arrows indicate the cracks along grain boundaries and the delaminations in grains, respectively.

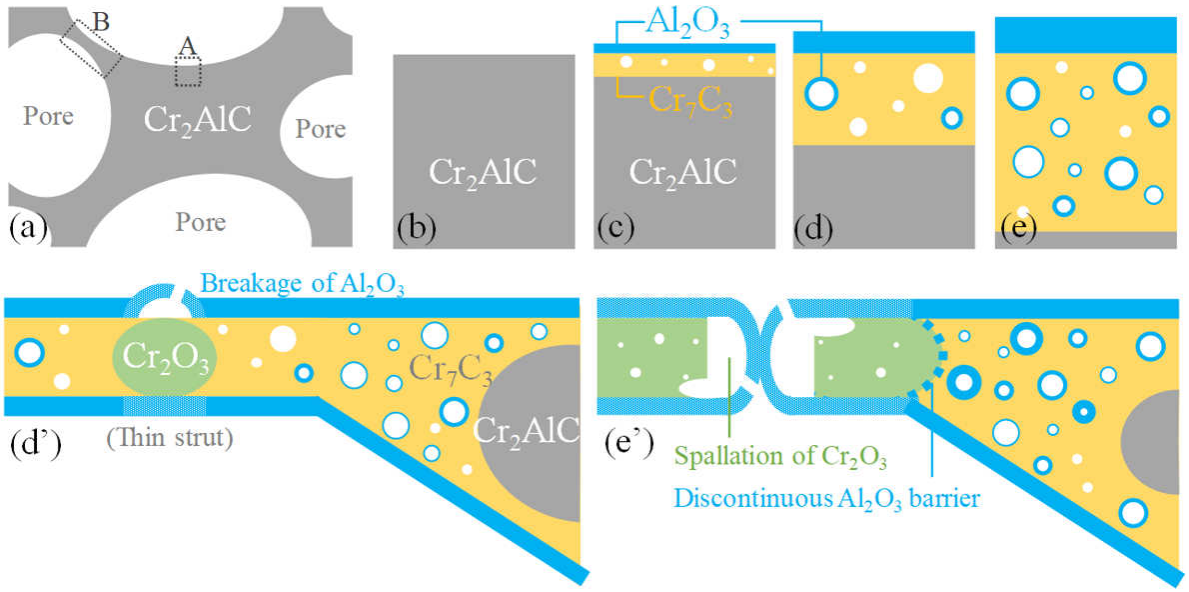

Figure 7 Oxidation mechanism of porous Cr_2AlC: (a) General view, (b)-(e) oxidation process on the surface of Cr_2AlC (e.g. area A in (a)), and (d')(e') oxidation process around thin strut (e.g. area B in (a), corresponding stage to (d) and (e)).

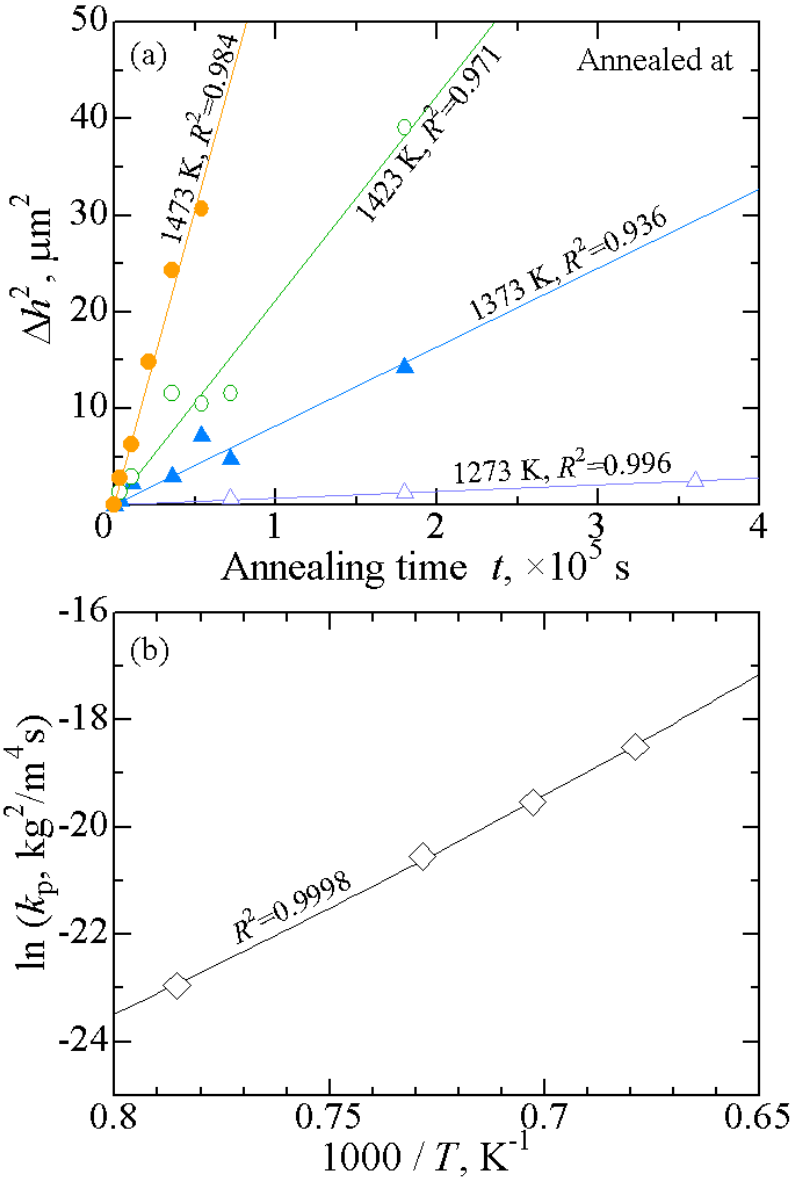

Figure 8 Al_2O_3 growth on porous Cr_2AlC oxidised under different conditions: (a) Approximations by the parabolic law and (b) Arrhenius plot of oxidation constant.

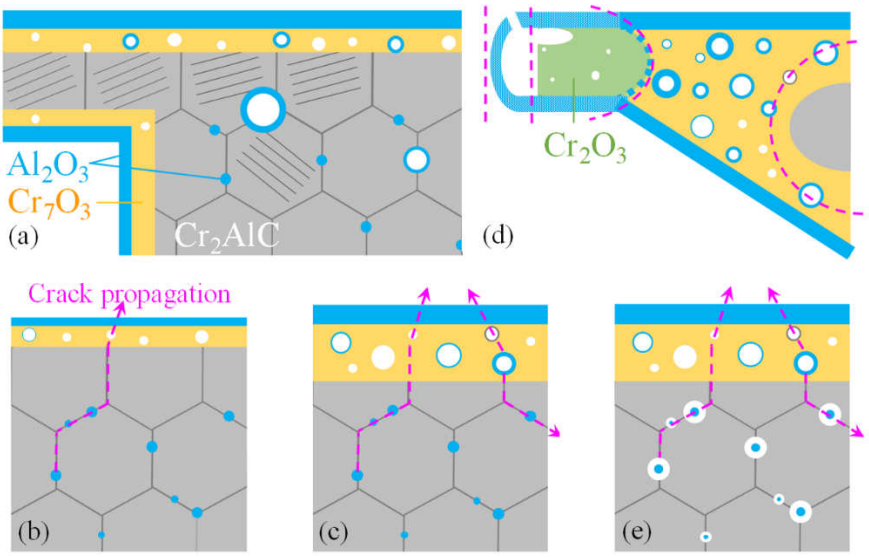

Figure 9 Fracture mode with crack propagation path in oxidised porous Cr_2AlC: (a) Al_2O_3 particles at the grain boundaries and transgranular fractures with delaminations (shown as striped patterns) in the constrained grains, (b) intergranular fracture in a slightly-oxidised sample, (c) in a more oxidised sample, (d) in an excessively-oxidised sample (corresponding to Fig. 7(e')), and (e) intergranular fracture with dimple formations at high temperatures. The dashed lines indicate possible crack propagation paths.

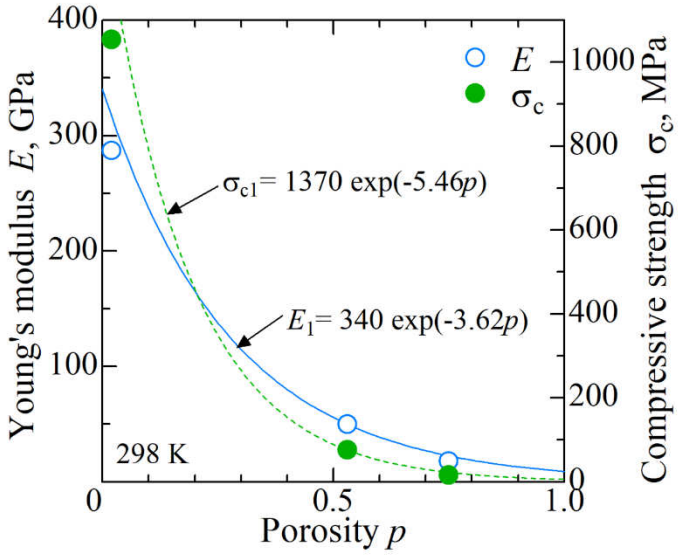

Figure 10 Mechanical properties of Cr_2AlC with different porosities obtained in the uniaxial compression test at 298 K and the approximations.

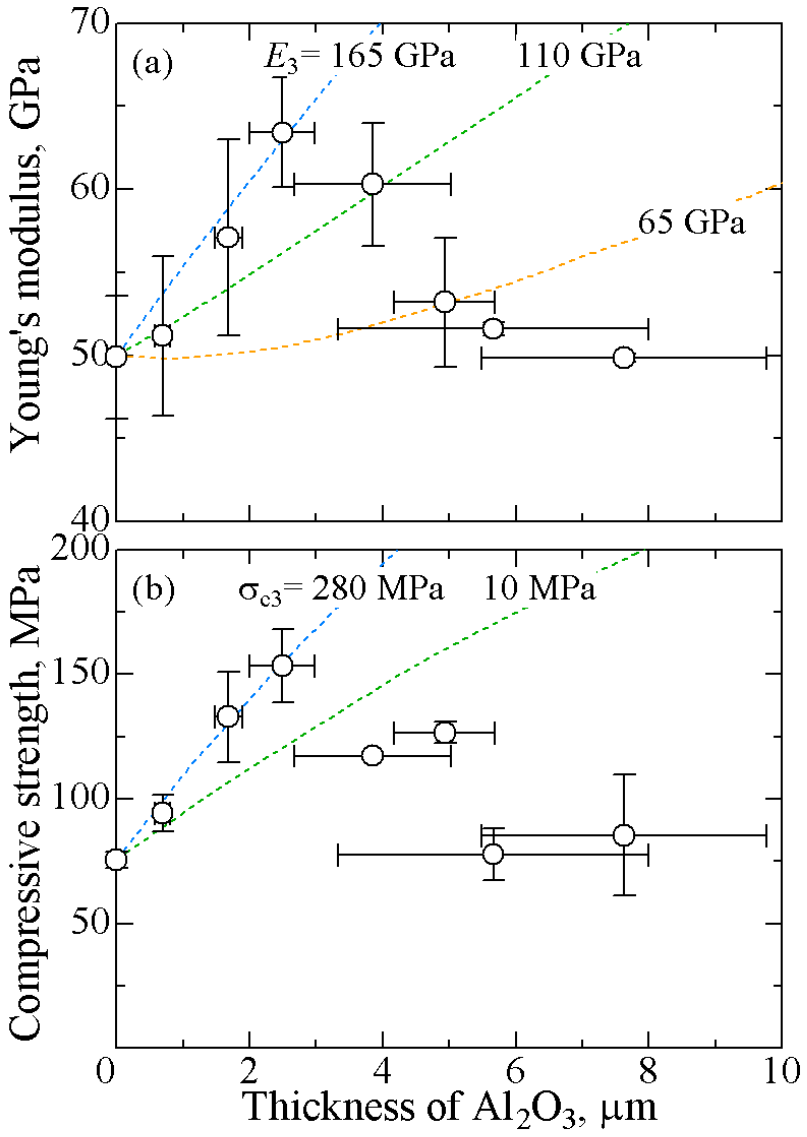

Figure 11 Predictions of mechanical properties of oxidised porous Cr2AlC at 298 K: (a) Young's modulus and (b) compressive strength.

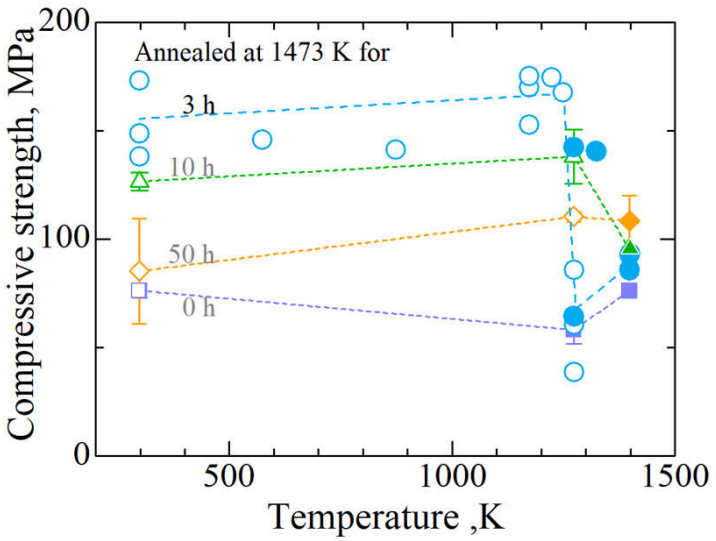

Figure 12 Compressive strength of porous Cr_2AlC annealed at 1473 K for 3 h as a function of temperature from 298 K to 1398 K. The strength of porous Cr_2AlC annealed at 1473 K for 0, 10, and 50 h are shown for comparison. The open and filled symbols represent brittle fracture and plastic deformation, respectively.

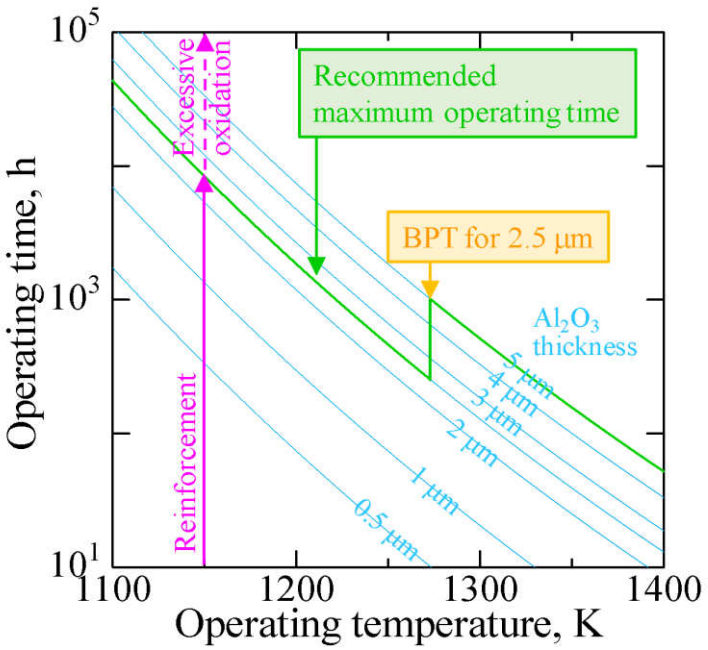

Figure 13 Recommended operating condition with Al_2O_3 thickness. The optimum Al_2O_3 thickness is assumed to be 2.5 μm for the temperature $T \leq 1273$ K and 5 μm for $T \geq 1273$ K, respectively, whilst the BRT (the brittle-to-plastic transition temperature) is 1273 K for the Al_2O_3 thickness of 2.5 μm.

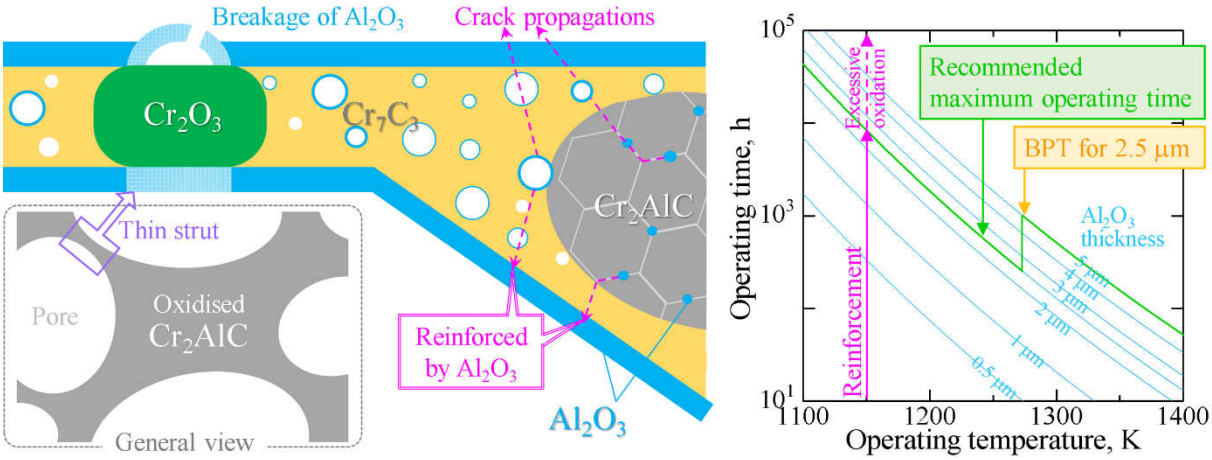

Graphical Abstract